Analysis of Electromagnetic Parameters of Hybrid Externally Excited Synchronous Motors for Electric Vehicle Applications

Duc-Quang Nguyen

Faculty of Electrical Engineering, Electric Power University, Vietnam
quangndhtd@epu.edu.vn

Linh Dinh Hai

Faculty of Electromechanical Engineering, Vietnam National University of Forestry, Vietnam
hailinhdinh1512@gmail.com

Dinh Bui Minh

School of Electrical and Electronic Engineering, Hanoi University of Science and Technology, Vietnam
dinh.buiminh@hust.edu.vn

Vuong Dang Quoc

School of Electrical and Electronic Engineering, Hanoi University of Science and Technology, Vietnam
vuong.dangquoc@hust.edu.vn (corresponding author)

ABSTRACT

This paper presents two different approaches to improve the electromagnetic torque and output power of the hybrid Externally Excited Synchronous Motor (EESM) applied to Electric Vehicles (EVs). An analytical approach is first considered to define the main parameters of the proposed machine. Based on the obtained results from the analytical model, the hybrid EESM is designed with different rotor shapes and step-skewing magnet segments to reduce the total losses and improve torque ripple. Then, Finite Element Analysis (FEA) is applied to compute and simulate electromagnetic parameters, such as the magnetic flux density, mean torque, and output power. The development of these two approaches is validated on an actual EESM machine and the agreement with the theory is shown.

Keywords-hybrid Electrically Excited Synchronous Motor (EESM); electromagnetic torque; output power; analytical method; Finite Element Method (FEM)

I. INTRODUCTION

Hybrid EESMs are widely used in industry and electric vehicles due to their good overload capability, high torque density, and efficiency. However, these electromagnetic parameters depend on the magnet rotor structure [1, 2]. Different approaches in EESM have been considered. Authors in [1] presented the skewing method to minimize the cogging torque and torque ripple. This way, the design is able to maintain the maximum available torque, which can improve the performance of the machine. In [2], a dual-rotor design of Permanent-Magnet (PM) machine was proposed to reduce the cogging torque. Both analytical and experimental results were presented to prove the effectiveness of the proposed design. In [3], an analytic model was proposed for hybrid EESM to

improve and analyze the torque density and magnetic flux density at the air gap. In [4], Finite Element Analysis (FEA) was extended to evaluate the electromagnetic performance of a proposed machine. The obtained results offer several advantages, including a simple and robust structure, high torque density, and low cogging torque. The results are compared with experimental tests and good agreement between simulation and measurement was reported. In [5], the Finite Element Method (FEM) was employed for PM Syncrhonous Motors (PMSMs) to find the optimal PM structure. Additionally, sub-group optimization and parallel computation were used to reduce the computational load, making the approach more efficient. In [6, 7], the performance of 3 different IPM rotor designs used by major car manufacturers was studied. The results of this study have practical

implications for the development of high-performance traction systems, specifically those used in hybrid electric vehicles.

Although the EESMs have been studied extensively, the minimization of losses (copper and iron) is more complex than that of other 3-phase motors, because the excitation current of the EESM will cause a saturated case in a high speed up to 20000 rpm. This is the reason why the study of the minimization of the losses of EESM drives is still a challenge for researchers and designers.

In this paper, an analytical approach is first considered to define the main parameters of the proposed machine. Based on the obtained results from the analytical model, a hybrid EESM is designed with different rotor shapes and step skewing magnet segments to reduce the total losses and improve torque ripple. Then, FEM is applied to compute and simulate electromagnetic parameters such as the magnetic flux density, mean torque, and output power. The development of this approach will be validated on an actual EESM of continuous rated power of 80kW (with peak power of 150kW and maximum speed of 20000 rpm) to show the agreement with the theory.

II. MODELING OF EESM DESIGN

The topology structure of the EESM design is shown in Figure 1. The topology is built to combine the analytical calculations in MATLAB with the FEM into one program. The process is divided into 3 main parts: analytical calculation, export drawing, and magnetic simulation. The analytical calculation is first computed in MATLAB and the obtained results, a detailed rotor and stator laminations, will be exported to cad files. Finally, they will be coupled to the simulation environment of FEM via the program interface developed by Matlab GUI.
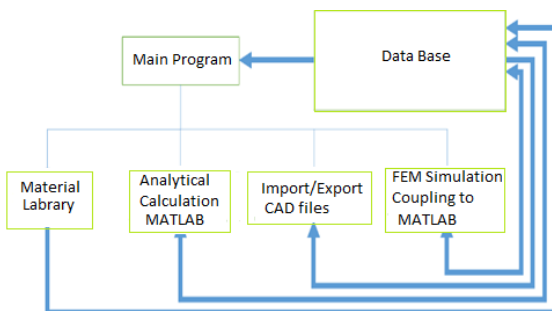

Fig. 1.   Topology structure of EESM design.

The topology structure shows the basic sizes (such as rotor and stator diameters, the lengths of rotor, airgap, and stator, and rotor and stator slots) of the proposed machine which need to be defined for the calculation process, i.e. performance specifications, limits of material properties, and temperature rise. However, there are some cases of machine designs already existing in the database. So, the properties of material components should be changed in order to minimize the total losses with technical constraints of the everage torque and output power. The geometry parameters of the stator and rotor are calculated by the process shown in Figure 2.
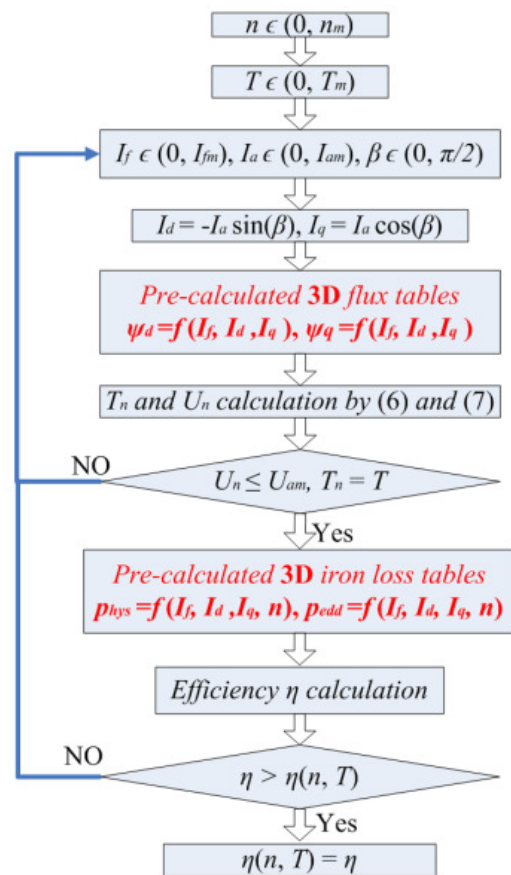

Fig. 2.   The calculation algorithm.

If the rotor diameter D is assumed to be equal to the rotor length L of the EESM, the electromagnetic torque (Nm) can be defined as [16-18]:

$$T = \frac{\pi}{4}.D^2.L_S.TRV \ (Nm) \tag{1}$$

where L_S is the length of core (m) and the TRV is the volume density (Nm/m^3), which can be expressed as [17, 18]:

$$TRV = \frac{\pi}{\sqrt{2}}k_{W1}A.B \ (Nm/m^3) \tag{2}$$

$$A = \frac{2m.N_{ph}I}{\pi D} \ (A/m) \tag{3}$$

Based on the general expression in (1) and in order to compute the electromagnetic torque and the output power at a synchronous speed, the phasor diagram presenting a salient-pole EESM machine with the reactance components X_d and X_q is shown in Figure 3, where X_d and X_q are the d- and q- axis reactances, and I_d and I_q are the d- and q- current components. The terms $I_q X_q$ and $I_d X_d$ are the voltage drops aligned along the d- and q-axes. The diagram is herein only presented for phase A. It is divided into two parts: the electrical voltage and current quantities are on the left side of the phasor diagram, and the magnetic flux linkages are on the right side. Generally, the magnetic flux linkages are usually neglected [12], however it can be considered as a physical reality that rotates in space.
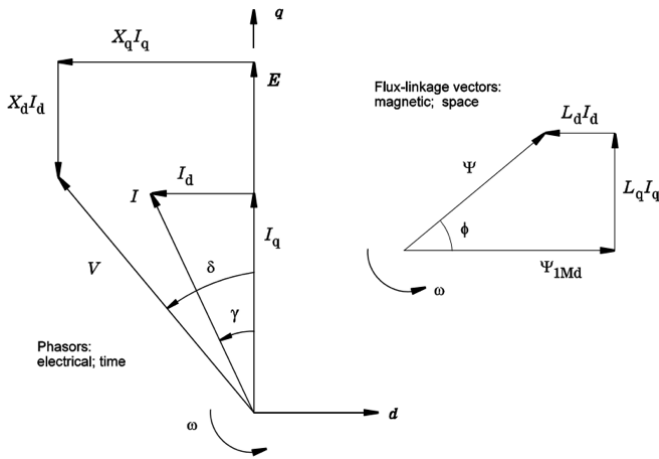
Fig. 3.   Phasor diagram of the EESM.

The physical orientation of a flux can be represented using a space vector, which is a mathematical construct that describes the magnitude and the direction of a physical quantity in 3-dimensional space. In the context of electromagnetism, space vectors are often used to represent the orientation of magnetic fields. The electromagnetic torque is computed as [8-11]:

$$T = \frac{mp}{\omega}[EI_d + I_d I_q \omega (L_d - L_q), \tag{4}$$

where I_d and I_q can be expressed as:

$$I_d = -I \sin \gamma \quad \text{and} \quad I_q = -I \cos \gamma, \tag{5a-b}$$

where E is the electromagnetic force (EMF) and the products $L_d I_d$ and $L_q I_q$ are the d- and q-axis flux-linkages. The wound poles of a traditional PM machine are generally replaced by PMs. The d- axis is the direction of the magnetic flux produced by the rotor, while the q- axis shows the quadrature direction perpendicular to the d- axis. This means that the PMs are located inside the rotor and have different inductive properties along the d- and q- axes. This can result in differences in the permeability along these axes, which can affect the motor performance. In contrast, in an exterior-IPM motor, the PMs are located on the surface of the rotor. The PM-assisted reluctance motors are a motor type that uses both PMs and salient poles to generate torque.

III. THEORICAL BACKGROUND

The minimization of the total losses of an EESM is a significant challenge for designers because it requires determination of all system parameters. Additionally, implementing control strategies for an EESM is complex, and it can take a long time to find the minimum loss point due to the additional degree of freedom provided by the excitation current. To address these challenges, a new optimization approach called Copper-Losses Minimization Control (CLMC) has been proposed for the EESM. The goal of this approach is to control the motor so that copper losses are minimal at every operating point. It is important to note that copper losses constitute a significant portion (about 60%) of the total losses of the EESM drive, especially when the motor operates in the optimal control range. By minimizing copper losses in the motor, the efficiency of the EESM drive can be considerably improved. Thus, copper losses occur in the stator and excitation windings of the EESM and can be modeled through the stator and excitation resistances as follows [12-15]:

$$P_{Cu} = \frac{3}{2} R_s \left(i_d^2 + i_q^2 \right) + R_f' i_f'^2 \tag{6}$$

where R_s and R_f' are respectively the stator and excitation resistances. These parameters can be expressed via the change of temperature as [14, 15]:

$$R_s(T_1) = R_s(T_o)\left(1 + \alpha_R(T_1 - T_o)\right) \tag{7}$$

$$R_f'(T_f) = R_f'(T_o)\left(1 + \alpha_R(T_1 - T_o)\right) \tag{8}$$

where α_R is the material temperature coefficient at the reference temperature T_0. Its value is usually given at 20°C, e.g. for copper conductor $\alpha_R = 0.004041$ (1/K). If the constraints of the stator voltage and current are neglected, the expression of loss minimization becomes [12, 13]:

$$\underset{i_d, i_q, i_f'}{min} \, P_{Cu}\left(i_d, i_q, i_f'\right) s.t \, T_e\left(i_d, i_q, i_f'\right) = T_{e,ref} \tag{9}$$

It should be noted that the degree of freedom in the excitation current control for the EESM can make the problem of optimal control more challenging compared to loss minimization problems of other 3-phase machines, because the excitation current is not directly tied to the load. One challenge in the optimal control of EESMs is determining the optimal excitation current for a given load condition. This is because the excitation current affects both the electromagnetic torque and the iron and copper losses in the machine. Thus, an optimal control strategy needs to consider both torque and loss components to achieve the desired performance. Another challenge is the non-linear nature of the EESM. The machine response to changes in excitation current and load conditions may not be linear, and this can make it difficult to develop an accurate model for control purposes. Furthermore, the EESM may exhibit hysteresis effects due to the saturation in the magnetic core, which can further complicate the control problem. To overcome these challenges, advanced control techniques such as model predictive control, adaptive control, and neural network-based control may be used. These techniques can help optimize the excitation current for a given load condition, while also compensating for the non-linearities and hysteresis effects of the EESM.

IV. ANALYSIS OF ELECTROMAGNETIC PERFORMANCE

Based on the theory presented above, in this section, a practical EESM of 80kW rated power (with peak power of 150kW and maximum speed of 20000 rpm), applied to an electric car, BYD ATTO 3 model [16], is considered. The main parameters of the proposed machine are given in Table I. The cross section of stator and rotor laminations of the EESM (model BYD ATTO 3) of 150kW-16000 rpm is presented in Figure 4. The distribution of magnetic flux density along the air gap of the hybrid and normal EESM motors is presented in Figure 5. The obtained results show that the value of the magnetic flux density in the hybrid EESM motor is higher than that in the normal EESM motor, due to the flux-concentration

effect of the PM in the hybrid EESM. In the hybrid EESM, the PM is placed on the rotor surface, which causes the magnetic flux to be concentrated in the area around the PM, resulting in a higher magnetic flux density in the air gap compared to the normal EESM, which does not have a PM on the rotor. The higher magnetic flux density in the air gap of the hybrid EESM motor can lead to several benefits. It can increase the electromagnetic torque produced by the motor, resulting in higher performance. Figure 6 shows the torque and speed curves of the hybrid and normal EESM motors. With the imposed current of 10A, there is a difference in the average torque between the hybrid and normal EESM motors. The average torque of the normal EESM has a lower value than that of the EESM when the speed is lower than 7000 rpm.

TABLE I.   MAIN PARAMETERS OF THE CONSIDERED CAR

| Parameter	Value	Unit
BYD ATTO 3	2020	
Peak power	150	kW
Hairpin winding		
Stator assy weight	23.6	kg
Stator lamination weight	17.98	kg
Copper weight	5.388	kg
Stator assembly	6.36	kg
Copper	27.40	kg
Stator iron	8.30	kg
Cooling system (liquid cooling)		
Voltage	394	volt
Slot number	48	
Pole number	8	
Shaft diameter	60	mm
Rotor outer diameter	138	mm
Stator inner diameter	139.4	mm
Airgap length	0.7	mm
Stator stack length	140	mm
Rotor stack length	141.6	mm
Average stack	140.8	mm
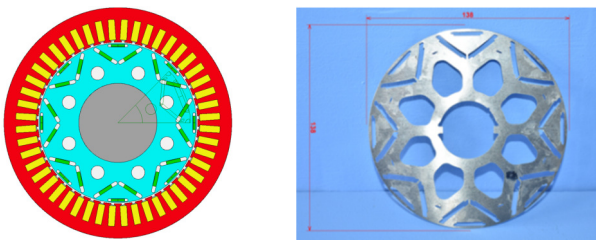
Fig. 4.   Cross section of stator and rotor laminations of EESM (BYD ATTO 3 model) of 150kW-16000 rpm.
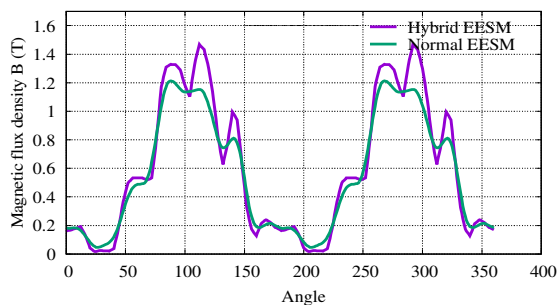

Fig. 5.   Magentic flux density distribution along the air gap of hybrid and normal EESM motors.
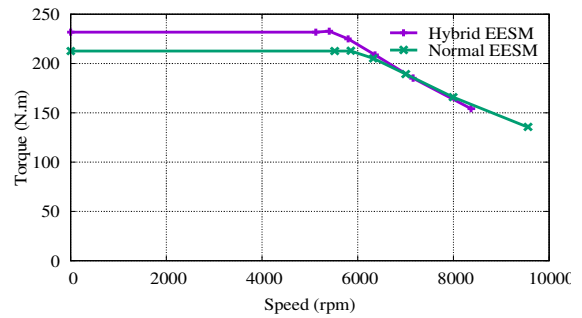

Fig. 6.   Comparison of average torque distribution of the two models (hybrid and normal EESM).

In addition to the evarate torque, the output power of the hybrid and normal EESM motor under the full range of speed is presented in Figure 7. The obtained results show that the output power of the hybrid EESM is improved in the higher-speed region, due to the presence of the PM on the rotor surface, which provides additional magnetic flux and improves the motor performance. The higher magnetic flux density in the air gap of the hybrid EESM results in a higher electromagnetic torque, as well as better output power at higher speeds. The detailed comparison of the parameters of hybrid and normal EESM is presented in Table II.

TABLE II.   PARAMETER COMPARISON OF NORMAL AND HYBRID EESM MOTORS

| Parameters	Hybrid EESM	Normal EESM	Unit
Maximum torque possible (DQ)	233.32	212.51	Nm
Average torque (virtual work)	234.9	211.79	Nm
Average torque (loop torque)	233.41	210.45	Nm
Torque ripple (MsVw)	28.235	7.6187	Nm
Torque ripple (MsVw) [%]	12.028	3.5959	%
Cogging torque ripple (Vw)	2.5773	0	Nm
Electromagnetic power	98327	88748	W
Input power	1.02E+05	92767	W
Output power	97681	88173	W
System efficiency	95.445	95.047	%
Armature DC copper loss	1938	1938	W
Field DC copper loss	2077	2082	W
Damper cage loss	10	10	W
Stator iron loss	541.7	540.8	W
Rotor iron loss	27.09	27.4	W
Wedge loss	7	7	W
Windage loss	7.035	7.035	W
Friction loss	8	8	W
Shaft loss	4.82E-08	5.06E-08	W
Total losses	4591	4595	W
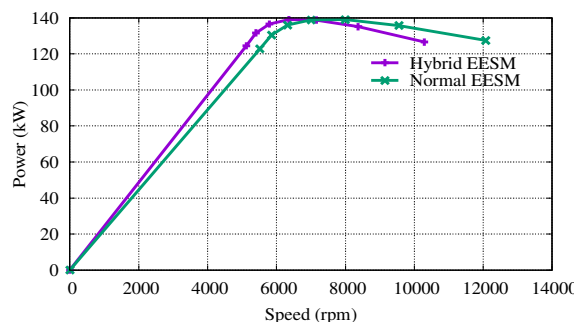
Fig. 7.   Power distribution of the two models (hybrid and normal EESM).

V. CONCLUSION

The current paper has analyzed and compared the magnetic flux density, average torque, and output power of two types of electric motors (hybrid and normal EESM) used in electric vehicle applications. Once of the significant contributions of the current study is that it highlights the improvement in the magnetic flux density, average torque, and output power of the hybrid EESM motor compared to the normal EESM motor over a wide range of speeds. The improved performance of the hybrid EESM motor is likely caused by its unique design and construction, which combines features of both the PMSM and EESM.

REFERENCES

[1] W. Zhao, T. A. Lipo, and B.-I. Kwon, "Torque Pulsation Minimization in Spoke-type Interior Permanent Magnet Motors With Skewing and Sinusoidal Permanent Magnet Configurations," *IEEE Transactions on Magnetics*, vol. 51, no. 11, pp. 1–4, Aug. 2015, https://doi.org/10.1109/TMAG.2015.2442977.

[2] E. Yıldırız, M. Güleç, and M. Aydın, "An Innovative Dual-Rotor Axial-Gap Flux-Switching Permanent-Magnet Machine Topology With Hybrid Excitation," *IEEE Transactions on Magnetics*, vol. 54, no. 11, pp. 1–5, Aug. 2018, https://doi.org/10.1109/TMAG.2018.2848878.

[3] Y. Liu, Z. Zhang, and X. Zhang, "Design and Optimization of Hybrid Excitation Synchronous Machines With Magnetic Shunting Rotor for Electric Vehicle Traction Applications," *IEEE Transactions on Industry Applications*, vol. 53, no. 6, pp. 5252–5261, Aug. 2017, https://doi.org/10.1109/TIA.2017.2720671.

[4] W. Li, T. W. Ching, and K. T. Chau, "Design and analysis of a new parallel-hybrid-excited linear vernier machine for oceanic wave power generation," *Applied Energy*, vol. 208, pp. 878–888, Dec. 2017, https://doi.org/10.1016/j.apenergy.2017.09.061.

[5] X. Liu, Q. Lin, and W. Fu, "Optimal Design of Permanent Magnet Arrangement in Synchronous Motors," *Energies*, vol. 10, no. 11, Nov. 2017, Art. no. 1700, https://doi.org/10.3390/en10111700.

[6] Y. Yang *et al.*, "Design and Comparison of Interior Permanent Magnet Motor Topologies for Traction Applications," *IEEE Transactions on Transportation Electrification*, vol. 3, no. 1, pp. 86–97, Mar. 2017, https://doi.org/10.1109/TTE.2016.2614972.

[7] A. Wang, Y. Jia, and W. L. Soong, "Comparison of Five Topologies for an Interior Permanent-Magnet Machine for a Hybrid Electric Vehicle," *IEEE Transactions on Magnetics*, vol. 47, no. 10, pp. 3606–3609, Jul. 2011, https://doi.org/10.1109/TMAG.2011.2157097.

[8] T. Ding, N. Takorabet, F.-M. Sargos, and X. Wang, "Design and Analysis of Different Line-Start PM Synchronous Motors for Oil-Pump Applications," *IEEE Transactions on Magnetics*, vol. 45, no. 3, pp. 1816–1819, Mar. 2009, https://doi.org/10.1109/TMAG.2009.2012772.

[9] A. Khlaief, M. Boussak, and M. Gossa, "Model Reference Adaptive System Based Adaptive Speed Estimation for Sensorless Vector Control with Initial Rotor Position Estimation for Interior Permanent Magnet Synchronous Motor Drive," *Electric Power Components and Systems*, vol. 41, no. 1, pp. 47–74, Jan. 2013, https://doi.org/10.1080/15325008.2012.732657.

[10] T. H. Manh, D. B. Minh, T. P. Minh, and V. D. Quoc, "Investigation of the Influence of Skewed Slots and Degmagnetization Effects to Line Start Permanent Magnet Assistance Synchronous Reluctance Motors," *Engineering, Technology & Applied Science Research*, vol. 13, no. 1, pp. 9807–9811, Feb. 2023, https://doi.org/10.48084/etasr.5307.

[11] T. A. Huynh and M.-F. Hsieh, "Performance Analysis of Permanent Magnet Motors for Electric Vehicles (EV) Traction Considering Driving Cycles," *Energies*, vol. 11, no. 6, Jun. 2018, Αρτ. No. 1385, https://doi.org/10.3390/en11061385.

[12] W. L. Soong and N. Ertugrul, "Field-weakening performance of interior permanent-magnet motors," *IEEE Transactions on Industry Applications*, vol. 38, no. 5, pp. 1251–1258, Sep. 2002, https://doi.org/10.1109/TIA.2002.803013.

[13] P. Guglielmi, B. Boazzo, E. Armando, G. Pellegrino, and A. Vagati, "Permanent-Magnet Minimization in PM-Assisted Synchronous Reluctance Motors for Wide Speed Range," *IEEE Transactions on Industry Applications*, vol. 49, no. 1, pp. 31–41, Jan. 2013, https://doi.org/10.1109/TIA.2012.2229372.

[14] X. Liu, H. Chen, J. Zhao, and A. Belahcen, "Research on the Performances and Parameters of Interior PMSM Used for Electric Vehicles," *IEEE Transactions on Industrial Electronics*, vol. 63, no. 6, pp. 3533–3545, Jun. 2016, https://doi.org/10.1109/TIE.2016.2524415.

[15] J. Wang, X. Yuan, and K. Atallah, "Design Optimization of a Surface-Mounted Permanent-Magnet Motor With Concentrated Windings for Electric Vehicle Applications," *IEEE Transactions on Vehicular Technology*, vol. 62, no. 3, pp. 1053–1064, Mar. 2013, https://doi.org/10.1109/TVT.2012.2227867.

[16] "BYD Yuan Plus," *Chinamobil*. https://www.chinamobil.ru/eng/byd/yuan-plus/.

[17] D. B. Minh, L. D. Hai, T. L. Anh, and V. D. Quoc, "Electromagnetic Torque Analysis of SRM 12/8 by Rotor/Stator Pole Angle," *Engineering, Technology & Applied Science Research*, vol. 11, no. 3, pp. 7187–7190, Jun. 2021, https://doi.org/10.48084/etasr.4168.

[18] D. B. Minh, L. D. Hai, T. L. Anh, and V. D. Quoc, "Electromagnetic Torque Analysis of SRM 12/8 by Rotor/Stator Pole Angle," *Engineering, Technology & Applied Science Research*, vol. 11, no. 3, pp. 7187–7190, Jun. 2021, https://doi.org/10.48084/etasr.4168.